JCTC Journal of Chemical Theory and Computation

E2 and S_N2 Reactions of $X^- + CH_3CH_2X$ (X = F, Cl); an *ab Initio* and DFT Benchmark Study

A. Patrícia Bento,[†] Miquel Solà,[‡] and F. Matthias Bickelhaupt*,[†]

Department of Theoretical Chemistry and Amsterdam Center for Multiscale Modeling, Scheikundig Laboratorium der Vrije Universiteit, De Boelelaan 1083, NL-1081 HV Amsterdam, The Netherlands, and Institut de Química Computacional, Universitat de Girona, Campus Montilivi, E-17071 Girona, Catalonia, Spain

Received November 20, 2007

Abstract: We have computed consistent benchmark potential energy surfaces (PESs) for the *anti*-E2, *syn*-E2, and S_N2 pathways of $X^- + CH_3CH_2X$ with X = F and Cl. This benchmark has been used to evaluate the performance of 31 popular density functionals, covering local-density approximation, generalized gradient approximation (GGA), meta-GGA, and hybrid density-functional theory (DFT). The *ab initio* benchmark has been obtained by exploring the PESs using a hierarchical series of *ab initio* methods [up to CCSD(T)] in combination with a hierarchical series of Gaussian-type basis sets (up to aug-cc-pVQZ). Our best CCSD(T) estimates show that the overall barriers for the various pathways increase in the order *anti*-E2 (X = F) < S_N2 (X = F) < S_N2 (X = Cl) ∼ *syn*-E2 (X = F) < *anti*-E2 (X = Cl) < *syn*-E2 (X = Cl). Thus, *anti*-E2 dominates for $F^- + CH_3CH_2F$, and S_N2 dominates for $Cl^- + CH_3CH_2Cl$, while *syn*-E2 is in all cases the least favorable pathway. Best overall agreement with our *ab initio* benchmark is obtained by representatives from each of the three categories of functionals, GGA, meta-GGA, and hybrid DFT, with mean absolute errors in, for example, central barriers of 4.3 (OPBE), 2.2 (M06-L), and 2.0 kcal/mol (M06), respectively. Importantly, the hybrid functional BHandH and the meta-GGA M06-L yield incorrect trends and qualitative features of the PESs (in particular, an erroneous preference for S_N2 over the *anti*-E2 in the case of $F^- + CH_3CH_2F$) even though they are among the best functionals as measured by their small mean absolute errors of 3.3 and 2.2 kcal/mol in reaction barriers. OLYP and B3LYP have somewhat higher mean absolute errors in central barriers (5.6 and 4.8 kcal/mol, respectively), but the error distribution is somewhat more uniform, and as a consequence, the correct trends are reproduced.

1. Introduction

Base-induced elimination (E2) and nucleophilic substitution (S_N2) constitute two fundamental types of chemical reactions that play an important role in organic synthesis.[1] E2 elimination is, in principle, always in competition with S_N2 substitution, and the two pathways may occur as unwanted side reactions of each other (see Scheme 1). Gas-phase experiments have enabled the study of the intrinsic reactivity of reaction systems without the interference of solvent molecules. The resulting insights, in turn, can also shed light on the nature of the E2 and S_N2 reactions in solution, in

Scheme 1. E2 and S_N2 Reactions

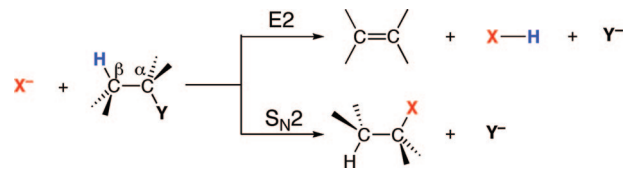

* Corresponding author fax: +31-20-59 87629; e-mail: FM.Bickelhaupt@few.vu.nl.
[†] Scheikundig Laboratorium der Vrije Universiteit.
[‡] Universitat de Girona.

10.1021/ct700318e CCC: $40.75
Published on Web 05/24/2008

Scheme 2. E2 and S_N2 Pathways for $X^- + CH_3CH_2X$

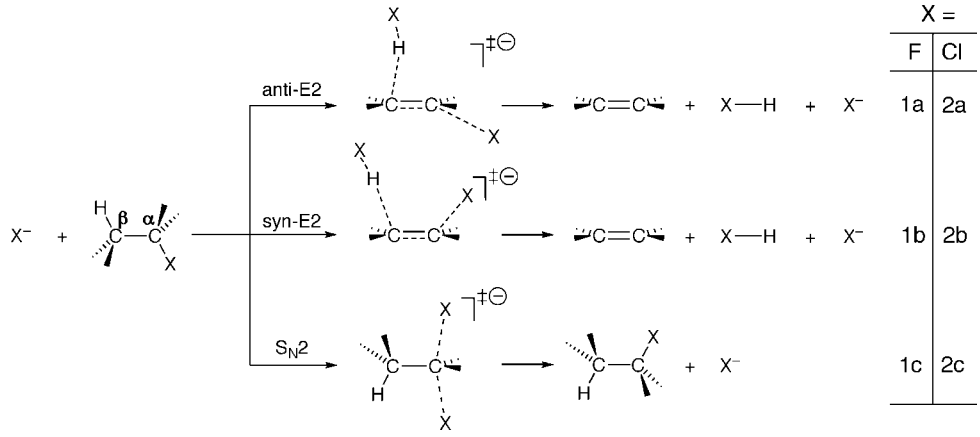

particular the effect of the solvent, by comparing the gas-phase[2] results with those of condensed-phase[3] experiments. The various experimental investigations have over the years been augmented by an increasing number of theoretical studies, which provide a detailed description of the stationary points and the potential energy surfaces (PESs) that determine the feasibility of the various competing E2 and S_N2 reaction channels.[4]

The purpose of the present study is 2-fold. First, we wish to obtain reliable benchmarks for the PESs of the E2 and S_N2 reactions of $F^- + CH_3CH_2F$ as well as $Cl^- + CH_3CH_2Cl$ (see reactions 1 and 2 in Scheme 2). Note that E2 eliminations can in principle proceed via two stereochemical, different pathways, namely, with the base and the β-proton anti- (*anti*-E2) and syn-periplanar (*syn*-E2) with respect to the leaving group (compare reactions a and b, respectively, in Scheme 2). This is done by exploring for both reaction systems the PESs of each of the three reaction mechanisms with a hierarchical series of *ab initio* methods [HF, MP2, MP4, CCSD, and CCSD(T)] in combination with a hierarchical series of Gaussian-type basis sets of increasing flexibility [up to quadruple-ζ + diffuse functions for reactions involving F and up to (triple+*d*)-ζ + diffuse functions for reactions involving Cl]. Our purpose is to provide a consistent set of *ab initio* PES data for accurately estimating trends associated with going from $F^- + CH_3CH_2F$ to $Cl^- + CH_3CH_2Cl$ as well as along *anti*-E2, *syn*-E2, and S_N2 pathways.

A second purpose is to evaluate and validate the performance of several popular density functionals for describing the above elimination and nucleophilic substitution reactions (see Scheme 2) against our *ab initio* benchmark PESs for the six model reactions. Although the *ab initio* approach is satisfactory in terms of accuracy and reliability, it is at the same time prohibitively expensive if one wishes to study more realistic model reactions involving larger nucleophiles and substrates. Thus, a survey of density functionals serves to validate one or more of these density functional theory (DFT) approaches as a computationally more efficient alternative to high-level *ab initio* theory in future investigations. A general concern associated with the application of DFT to the investigation of chemical reactions is its notorious tendency to underestimate activation energies.[5] Thus, we arrive at a ranking of density functional approaches in terms of the accuracy with which they describe the PES of our model reaction, in particular, the activation energy. We focus on the overall activation energy, that is, the difference in energy between the TS and the separate reactants,[6] as well as the central barrier, that is, the difference in energy between the TS and the reactant complex. Previous studies have shown that S_N2 reaction profiles obtained with OLYP and B3LYP agree satisfactorily with highly correlated *ab initio* benchmarks.[5c,7] Merrill et al.[4g] have shown that B3LYP in combination with the aug-cc-pVDZ basis set performs reasonably well for the E2 and S_N2 reactions of $F^- + CH_3CH_2F$ with deviations from G2+ of up to 3.5 kcal/mol but that it fails in locating the transition state associated with the *anti*-E2 elimination. Guner et al.[7g] have also shown that OLYP and O3LYP give comparable results to B3LYP and that these functionals work well for organic reactions. Very recently, Truhlar and co-worker[7h] have carried out an exhaustive performance analysis of various density functionals for describing barrier heights which shows that, for closed-shell S_N2 reactions, M06 and M06-2X perform best, followed by PBEh and M05-2X. B3LYP is also found to work reasonably well.

2. Methods

2.1. DFT Geometries and Potential Energy Surfaces. All DFT calculations were done with the Amsterdam Density Functional (ADF) program developed by Baerends and others.[8] Geometry optimizations have been carried out with the OLYP[9] density functional, which yields robust and accurate geometries.[7a] This density functional was used in combination with the TZ2P basis set, in which the molecular orbitals were expanded in a large uncontracted set of Slater-type orbitals (STOs) containing diffuse functions, and is of triple-ζ quality, being augmented with two sets of polarization functions: 2p and 3d on hydrogen and 3d and 4f on carbon, fluorine, and chlorine. The core shells of carbon (1s), fluorine (1s), and chlorine (1s2s2p) were treated by the frozen-core approximation.[8b,10] An auxiliary set of s, p, d, f, and g STOs was used to fit the molecular density and to represent the Coulomb and exchange potentials accurately in each self-consistent field (SCF) cycle. All stationary points

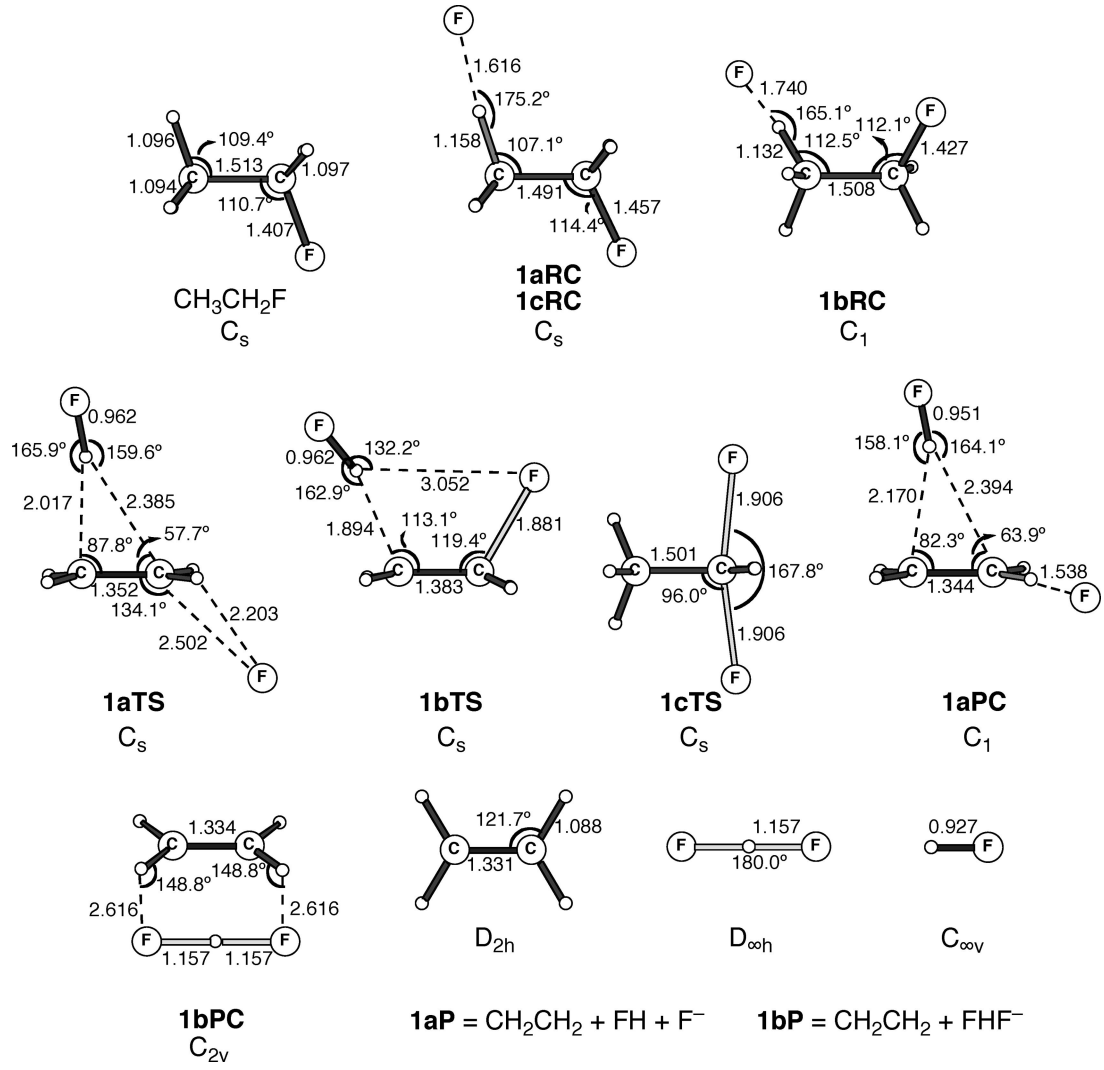

Figure 1. Geometries (in Å, deg) of stationary points along the potential energy surfaces for the *anti*-E2, *syn*-E2, and S_N2 reactions of $F^- + CH_3CH_2F$ (reaction 1), computed at OLYP/TZ2P.

were confirmed to be equilibrium structures (no imaginary frequencies) or a transition state[11] (one imaginary frequency) through vibrational analysis.[12]

In addition, based on OLYP/TZ2P geometries, we have computed the relative energies of stationary points along the PES for several density functionals: the local-density approximation (LDA) functional VWN;[13] the generalized gradient approximation (GGA) functionals BP86,[14] BLYP,[9b,14a] PW91,[15] PBE,[16] RPBE,[17] revPBE,[18] FT97,[19] HCTH/93,[20] HCTH/120,[21] HCTH/147,[21] HCTH/407,[22] BOP,[14a,23] and OPBE;[9a,16] the meta-GGA functionals PKZB,[24] VS98,[25] BLAP3,[26] OLAP3,[9a,26] TPSS,[27] and M06-L;[28] and the hybrid functionals B3LYP,[9b,29] O3LYP,[30] KMLYP,[31] BHandH,[32] mPBE0KCIS,[33] mPW1K,[34] M05,[35] M05-2X,[36] M06,[7h,37] and M06-2X.[7h,37] For technical reasons (i.e., frozen-core approximation and potentials in ADF are not available for all functionals), the energies obtained with these functionals were computed with an *all-electron* TZ2P basis set (ae-TZ2P) and in a post-SCF manner, that is, using the electron density obtained at OLYP/ae-TZ2P. This approximation has been extensively tested and has been shown to introduce an error in the computed energies of only a few tenths of a kilocalorie per mole.[38]

2.2. *Ab Initio* Potential Energy Surfaces. On the basis of the OLYP/TZ2P geometries, energies of the stationary points were computed in a series of single-point calculations with the program package Gaussian[39] using the following hierarchy of quantum chemical methods: Hartree−Fock (HF), Møller−Plesset perturbation theory[40] through the second order (MP2) and fourth order (MP4),[41] and coupled-cluster theory[42] with single and double excitations (CCSD)[43] and triple excitations treated perturbatively [CCSD(T)].[44] At each level of theory, we used Dunning's[45] augmented correlation consistent polarized valence basis sets of double-, triple-, and quadruple-ζ quality, that is, aug-cc-pVDZ, aug-cc-pVTZ, and aug-cc-pVQZ for the reactions involving F, and the modified second-row basis sets aug-cc-pV(D+*d*)Z and aug-cc-pV(T+*d*)Z for the reactions involving Cl (limitations of our computational resources prevented us from carrying out calculations with the aug-cc-pV(Q+*d*)Z basis set for the latter reactions). Furthermore, using eq 7 of ref 46, we have extrapolated the CCSD(T) energies to the complete basis set (CBS) values CBS-23 (i.e., based on aug-cc-pVDZ and aug-cc-pVTZ values for reactions involving F and aug-cc-pV(D+*d*)Z and aug-cc-pV(T+*d*)Z values for reactions involving Cl) and CBS-34 (i.e., based on aug-cc-

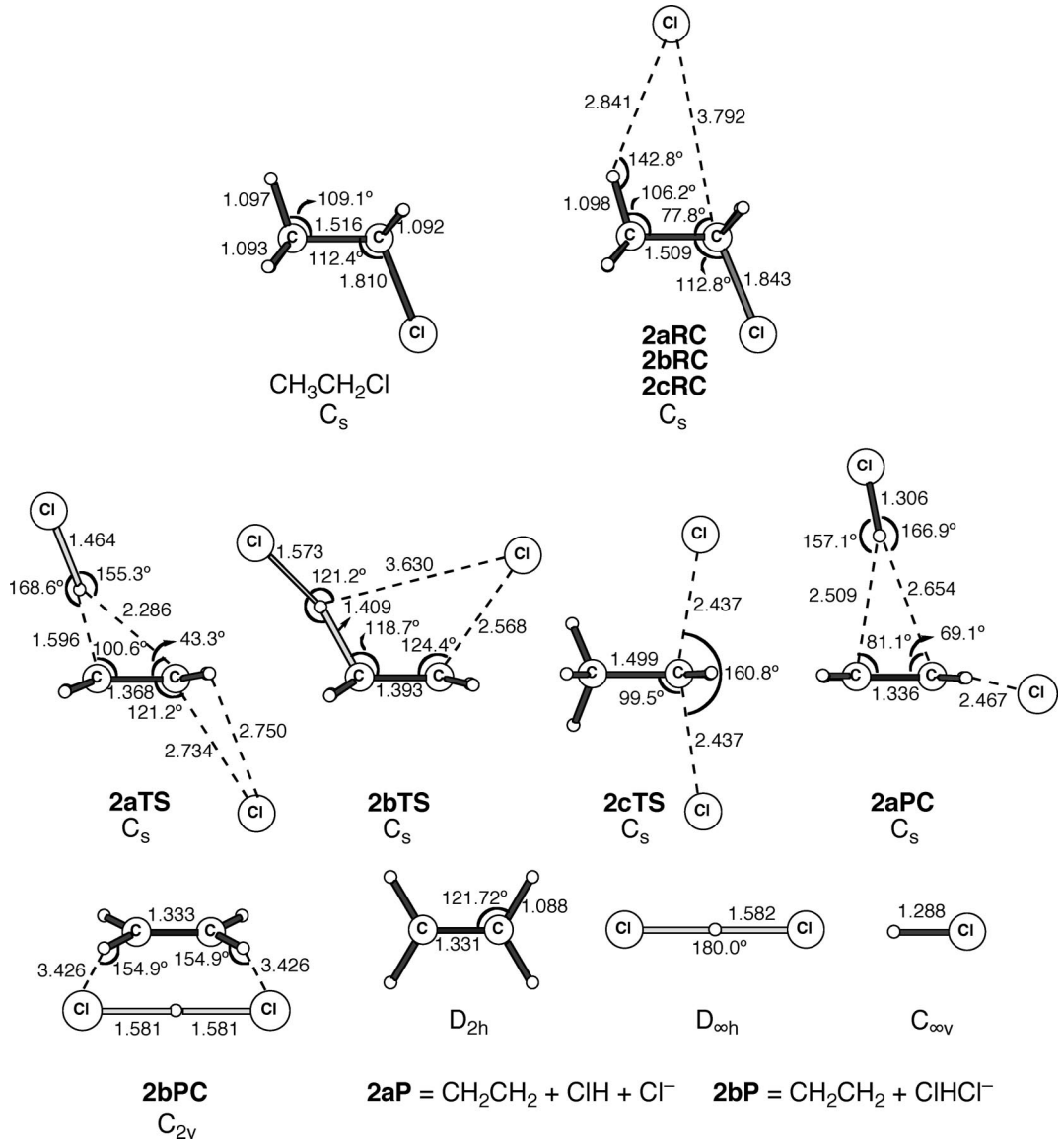

Figure 2. Geometries (in Å, deg) of stationary points along the potential energy surfaces for the *anti*-E2, *syn*-E2, and S_N2 reactions of $Cl^- + CH_3CH_2Cl$ (reaction 2), computed at OLYP/TZ2P.

pVTZ and aug-cc-pVQZ values, only for the reactions involving F).

3. Results and Discussion

3.1. Geometries of Stationary Points and Reaction Paths. First, we examine the geometries of stationary points along the reaction coordinate of *anti*-E2, *syn*-E2, and S_N2 reactions of $F^- + CH_3CH_2F$ and $Cl^- + CH_3CH_2Cl$. Previous studies have shown that the GGA functional OLYP is numerically robust and agrees well with available experimental and CCSD(T) geometries.[7a] Therefore, we choose OLYP in combination with the TZ2P basis set, to compute the geometries of the stationary points of our model reactions 1 and 2 (see Scheme 2). The resulting geometry parameters are collected in Figures 1 and 2, respectively (for full structural details, see Cartesian coordinates in Table S1 of the Supporting Information).

For both $F^- + CH_3CH_2F$ and $Cl^- + CH_3CH_2Cl$, the *anti*-E2, *syn*-E2, and S_N2 reactions proceed from the reactants via formation of a reactant complex (RC) toward the transition state (TS) and, finally, a product complex (PC). In the *anti*-E2 reactant complex, the base X^- binds to the $C^\beta-H$ bond that is anti to $C^\alpha-X$ with $X^-\cdots H^\beta$ distances of 1.616 and 2.841 Å in **1aRC** and **2aRC**, respectively (see Figures 1 and 2). The $C^\beta-H$ bond that participates in the hydrogen bond with the halide anion expands by 0.062 Å in **1aRC** (from 1.096 to 1.158 Å) and only very slightly, that is, by 0.001 Å, in **2aRC** (from 1.097 to 1.098) if compared to the isolated substrates CH_3CH_2F and CH_3CH_2Cl, respectively. In the *anti*-E2 transition states **1aTS** and **2aTS**, the elongation of the $C^\beta-H$ bonds further increases to 0.921 and 0.499 Å, respectively, again relative to the isolated substrates. The resulting product complexes **1aPC** and **2aPC** are composed of three rigid fragments, the conjugate acid HX, the olefin CH_2CH_2, and the leaving group X^-, which may eventually separate into products (**1aP** and **2aP**).

The *syn*-E2 elimination proceeds only in the case of $F^- + CH_3CH_2F$ via a separate reactant complex **1bRC** (see

Table 1. Relative Energies (in kcal/mol) of Stationary Points along the Reaction Coordinate for the *anti*-E2, *syn*-E2, and S_N2 Reactions of $F^- + CH_3CH_2F$, Computed at Several Levels of the *ab Initio* Theory

	anti-E2				*syn*-E2				S_N2	
method	**1aRC**	**1aTS**	**1aPC**	**1aP**	**1bRC**	**1bTS**	**1bPC**	**1bP**	**1cRC**	**1cTS**
					aug-cc-pVDZ					
HF	−10.49	4.81	0.12	16.77	−7.62	18.08	−28.00	−23.55	−10.49	8.71
MP2	−15.23	−1.77	−6.90	15.96	−11.01	4.86	−33.50	−27.40	−15.23	1.03
MP4	−15.64	−1.44	−6.03	17.10	−11.49	5.00	−31.68	−25.30	−15.64	−2.74
CCSD	−14.76	−0.30	−5.43	16.42	−10.92	8.38	−32.65	−26.70	−14.76	1.80
CCSD(T)	−15.81	−2.03	−7.16	16.11	−11.71	5.16	−33.88	−27.53	−15.81	−1.06
					aug-cc-pVTZ					
HF	−9.63	5.22	0.72	16.63	−7.05	18.42	−28.46	−24.25	−9.63	11.35
MP2	−14.69	−1.07	−6.06	16.48	−10.69	5.07	−33.81	−27.99	−14.69	3.56
MP4	−15.02	−0.88	−5.35	17.29	−11.08	5.05	−32.33	−26.27	−15.02	−0.20
CCSD	−14.13	0.56	−4.47	17.01	−10.54	8.89	−32.96	−27.29	−14.13	4.58
CCSD(T)	−15.17	−1.31	−6.28	16.51	−11.30	5.47	−34.30	−28.28	−15.17	1.56
					CBS[a]					
CCSD(T)	−15.27	−1.19	−6.17	16.74	−11.37	5.46	−34.28	−28.29	−15.27	1.55
					aug-cc-pVQZ					
HF	−9.58	5.12	0.57	16.31	−7.03	18.30	−28.43	−24.31	−9.58	11.50
MP2	−14.61	−1.25	−6.33	15.88	−10.60	4.93	−33.92	−28.30	−14.61	3.81
CCSD	−14.00	0.50	−4.61	16.45	−10.41	8.91	−32.98	−27.53	−14.00	4.97
CCSD(T)	−14.99	−1.33	−6.39	15.95	−11.12	5.54	−34.27	−28.49	−14.99	1.99
					CBS[b]					
CCSD(T)	−14.89	−1.27	−6.35	15.77	−11.00	5.68	−37.39	−28.60	−14.89	2.20

[a] These values were obtained from two-point fits (aug-cc-pVDZ and aug-cc-pVTZ) to eq 7 of ref 46. [b] These values were obtained from two-point fits (aug-cc-pVTZ and aug-cc-pVQZ) to eq 7 of ref 46.

Table 2. Relative Energies (in kcal/mol) of Stationary Points along the Reaction Coordinate for the *anti*-E2, *syn*-E2, and S_N2 Reactions of $Cl^- + CH_3CH_2Cl$, Computed at Several Levels of the *ab Initio* Theory

	anti-E2				*syn*-E2				S_N2	
method	**2aRC**	**2aTS**	**2aPC**	**2aP**	**2bRC**	**2bTS**	**2bPC**	**2bP**	**2cRC**	**2cTS**
					aug-cc-pV(D + d)Z					
HF	−9.33	26.88	10.03	17.93	−9.33	43.57	0.43	2.61	−9.33	9.06
MP2	−11.33	16.22	9.19	22.67	−11.33	29.51	−5.21	−1.50	−11.33	6.67
MP4	−11.45	16.22	8.08	21.30	−11.45	29.12	−5.01	−1.27	−11.45	4.39
CCSD	−10.98	18.95	8.30	20.40	−10.98	33.10	−4.12	−0.67	−10.98	6.43
CCSD(T)	−11.43	16.14	7.50	20.52	−11.43	29.17	−5.57	−1.86	−11.43	4.12
					aug-cc-pV(T + d)Z					
HF	−9.06	28.04	10.27	17.61	−9.06	44.99	0.99	3.04	−9.06	10.38
MP2	−11.06	17.90	10.80	23.86	−11.06	31.06	−4.42	−0.90	−11.06	8.22
CCSD	−10.64	20.97	9.90	21.38	−10.64	35.11	−3.15	0.07	−10.64	8.15
CCSD(T)	−11.10	17.92	9.17	21.58	−11.10	30.82	−4.90	−1.42	−11.10	5.70
					CBS[a]					
CCSD(T)	−11.07	18.18	9.77	22.16	−11.07	30.92	−4.85	−1.42	−11.07	5.81

[a] These values were obtained from two-point fits [aug-cc-pV(D + d)Z and aug-cc-pV(T+*d*)Z] to eq 7 of ref 46.

Figure 1). For $Cl^- + CH_3CH_2Cl$, all three elementary reactions (*anti*-E2, *syn*-E2, and S_N2) go via one and the same reactant complex, that is, **2aRC** = **2bRC** = **2cRC** (see Figure 2). In the *syn*-E2 transition states **1bTS** and **2bTS**, the C^β−H bonds are elongated by 0.798 and 0.312 Å and are oriented syn with respect to the C^α−X bond (see Figures 1 and 2). At variance with the *anti*-E2 pathway, the *syn*-E2 pathway leads to product complexes, **1bPC** and **2bPC**, that are composed of *two* rigid fragments: the leaving group microsolvated by the conjugate acid, XHX^-, and the olefin, CH_2CH_2. These product complexes are predestined to dissociate into the products $CH_2CH_2 + XHX^-$ (**1bP** and **2bP**).

S_N2 substitution proceeds for both $F^- + CH_3CH_2F$ and $Cl^- + CH_3CH_2Cl$, from the same reactant complex as the *anti*-E2 elimination (i.e., aRC = cRC). But now, the halide anion approaches to the backside of the α-methyl group of the substrate, which leads to the S_N2 transition states **1cTS** and **2cTS** in which a new X−C^α bond has been partially formed while simultaneously the old C^α−X bond has been elongated (see Figures 1 and 2). Note that, in our symmetric S_N2 model reactions, the nucleophile−C^α and C^α−leaving-group bonds are of the same length, namely, 1.906 and 2.437 Å in **1cTS** and **2cTS** (see Figures 1 and 2), and that the product complexes and products are identical to the corresponding reactant complexes and reactants.

3.2. *Ab Initio* Benchmark Potential Energy Surfaces. On the basis of the above OLYP/TZ2P geometries, we have computed our *ab initio* benchmark potential energy surfaces, which are summarized as relative energies in Tables 1 and 2 for reactions 1 and 2, respectively. The extrapolated CBS CCSD(T) values are also listed therein.

Table 3. Relative Energies (in kcal/mol) of Stationary Points along the Reaction Coordinate for the *anti*-E2, *syn*-E2, and S_N2 Reactions of $F^- + CH_3CH_2F$, Computed at Several Levels of the Density Functional Theory

	anti-E2				*syn*-E2				S_N2	
method	**1aRC**	**1aTS**	**1aPC**	**1aP**	**1bRC**	**1bTS**	**1bPC**	**1bP**	**1cRC**	**1cTS**
					LDA					
VWN	−28.23	−8.54	−13.84	26.01	−22.02	−12.50	−42.70	−35.13	−28.23	−13.67
					GGAs					
BP86	−22.19	−8.27	−12.55	16.97	−16.77	−7.51	−40.68	−35.87	−22.19	−9.33
BLYP	−22.23	−11.55	−15.08	13.55	−17.02	−8.66	−43.95	−38.71	−22.23	−11.27
PW91	−24.12	−9.58	−13.67	18.85	−18.66	−9.29	−42.15	−35.61	−24.12	−11.39
PBE	−23.79	−9.36	−13.49	18.48	−18.37	−8.98	−41.73	−35.43	−23.79	−10.73
RPBE	−21.79	−9.61	−13.49	14.89	−16.74	−7.39	−41.71	−35.87	−21.79	−8.56
revPBE	−21.37	−8.83	−12.85	15.00	−16.26	−6.85	−40.94	−35.73	−21.37	−7.91
FT97	−19.78	−6.54	−11.07	13.27	−14.08	−4.80	−37.86	−35.53	−19.78	−7.19
HCTH/93	−18.75	−7.32	−11.79	12.26	−13.98	−3.73	−40.42	−36.26	−18.75	−2.52
HCTH/120	−21.90	−9.85	−14.05	15.07	−16.92	−7.17	−42.93	−36.60	−21.90	−7.37
HCTH/147	−21.07	−8.93	−13.26	14.58	−16.10	−6.23	−42.13	−36.45	−21.07	−6.14
HCTH/407	−21.52	−10.56	−14.71	13.39	−16.74	−6.60	−44.06	−37.30	−21.52	−5.78
BOP	−19.67	−9.98	−13.56	11.28	−14.68	−6.01	−42.21	−38.16	−19.67	−7.66
OPBE	−18.68	−3.26	−8.45	15.78	−13.79	−2.07	−36.62	−32.69	−18.68	−0.22
OLYP	−20.01	−7.95	−12.49	12.85	−15.20	−4.93	−41.40	−36.41	−20.01	−4.16
					meta-GGAs					
PKZB	−19.16	−6.56	−9.65	14.74	−14.55	−3.93	−38.36	−32.85	−19.16	−7.27
VS98	−20.80	−13.42	−15.04	11.99	−16.25	−7.04	−43.88	−35.97	−20.80	−14.06
BLAP3	−18.54	−8.58	−12.38	12.58	−14.01	−2.47	−41.65	−36.58	−18.54	−4.88
OLAP3	−16.23	−4.62	−9.31	12.24	−12.13	1.57	−38.65	−33.88	−16.23	2.25
TPSS	−21.38	−5.26	−8.94	19.81	−16.28	−4.16	−37.83	−32.52	−21.38	−10.03
M06-L	−20.04	−1.23	−5.44	20.54	−15.33	1.68	−32.57	−27.78	−20.04	−2.95
					Hybrid Functionals					
B3LYP	−19.30	−5.38	−10.66	15.90	−14.50	−2.00	−40.32	−35.34	−19.30	−4.01
O3LYP	−18.12	−2.55	−7.97	16.52	−13.46	0.40	−38.06	−33.35	−18.12	0.24
KMLYP	−16.14	6.09	−2.78	23.69	−11.77	8.28	−33.82	−28.53	−16.14	7.54
BHandH	−19.68	3.90	−4.81	26.52	−14.87	3.86	−35.53	−29.15	−19.68	2.76
mPBE0KCIS	−19.57	−4.44	−10.63	16.89	−14.77	−1.77	−39.63	−33.94	−19.57	−1.15
mPW1K	−15.32	4.26	−3.38	20.37	−10.96	7.06	−33.31	−29.07	−15.32	6.24
M05	−18.68	−3.51	−8.73	18.54	−14.64	0.81	−38.03	−32.01	−18.68	−0.81
M05-2X	−14.53	0.99	−5.72	18.33	−10.30	3.85	−39.28	−34.27	−14.53	3.97
M06	−18.21	−2.21	−7.47	17.88	−13.96	1.14	−35.19	−30.59	−18.21	−0.35
M06-2X	−15.67	1.49	−5.62	18.37	−11.47	4.03	−37.77	−32.90	−15.67	5.82

First, we examine the PES obtained for the *anti*-E2 elimination of $F^- + CH_3CH_2F$. The energy of the respective reactant complex, **1aRC**, computed with our best basis set (aug-cc-pVQZ) ranges from −9.58 to −14.61 to −14.00 to −14.99 kcal/mol for HF, MP2, CCSD, and CCSD(T). Note that, due to large space requirements, full MP4 calculations for the QZ basis set were not possible. The three highest-level values are equal to each other within 1.0 kcal/mol (see Table 1). Similarly, the energy of the transition state, **1aTS**, computed again with our best basis set (aug-cc-pVQZ) varies from +5.12 to −1.25 to +0.50 to −1.33 kcal/mol for HF, MP2, CCSD, and CCSD(T), respectively. Thus, not unexpectedly, HF significantly overestimates the overall barrier, which is significantly reduced by the incorporation of Coulomb correlation into theoretical treatment. The inclusion of the triple excitations within the CCSD method further reduces the overall barrier by 1.8 kcal/mol. The three highest-level values are within a range of 1.8 kcal/mol. Furthermore, the CCSD(T) values are converged to the basis-set size (at aug-cc-pVQZ) to within a few hundreds of a kilocalorie per mole for the RC and the TS (see Table 1). Note that CBS CCSD(T) values do not differ much from the best pure values [CCSD(T)].

For the *anti*-E2 elimination of $Cl^- + CH_3CH_2Cl$, the energy of the reactant complex, **2aRC**, computed with our best basis set [now, with aug-cc-pV(T+*d*)Z] varies relatively little along the range of methods, that is ca. 2 kcal/mol, from −9.06 to −11.06 to −10.64 to −11.10 for HF, MP2, CCSD and CCSD(T), respectively (see Table 2). Now, our three highest-level values are equal to each other within 0.5 kcal/mol. At variance, the energy of the transition state, **2aTS**, depends more delicately on the level at which correlation is treated. This TS energy computed again with aug-cc-pV(T+*d*)Z varies from 28.04 to 17.90 to 20.97 to 17.92 kcal/mol along HF, MP2, CCSD, and CCSD(T), respectively. Note how HF dramatically overestimates the overall barrier, that is, by ca. 10 kcal/mol! Also note the substantial impact of including triple excitations in the CCSD approach, which reduced the overall barrier by an additional 3.0 kcal/mol. The three highest-level values are now distributed over a range of 3.1 kcal/mol (see Table 2).

Next, we examine the PES of the *syn*-E2 elimination of $F^- + CH_3CH_2F$. The energy of reactant complex **1bRC** computed with our best basis set (aug-cc-pVQZ) shows a similar behavior as that of the *anti*-E2 elimination. The energy of this RC varies from −7.03 to −10.60 to −10.41 to −11.12 kcal/mol for HF, MP2, CCSD, and CCSD(T), respectively, and the three highest-level values are within a range of less than a kcal/mol (see Table 1). In turn, the energy of the TS is more sensitive to the level at which correlation

Table 4. Relative Energies (in kcal/mol) of Stationary Points along the Reaction Coordinate for the *anti*-E2, *syn*-E2, and S_N2 Reactions of $Cl^- + CH_3CH_2Cl$, Computed at Several Levels of the Density Functional Theory

	anti-E2				*syn*-E2				S_N2	
method	**2aRC**	**2aTS**	**2aPC**	**2aP**	**2bRC**	**2bTS**	**2bPC**	**2bP**	**2cRC**	**2cTS**
					LDA					
VWN	−13.32	5.00	12.19	29.51	−13.32	11.45	−10.74	−7.11	−13.32	−4.64
					GGAs					
BP86	−10.66	7.21	8.80	20.08	−10.66	15.35	−11.23	−9.24	−10.66	−1.92
BLYP	−11.08	5.28	4.43	15.33	−11.08	14.04	−14.17	−11.93	−11.08	−3.69
PW91	−12.23	6.38	8.42	22.36	−12.23	14.22	−11.98	−8.56	−12.23	−3.24
PBE	−11.91	6.85	8.62	22.10	−11.91	14.75	−11.62	−8.49	−11.91	−2.43
RPBE	−11.20	7.78	6.85	18.45	−11.20	16.27	−12.47	−9.38	−11.20	−0.67
revPBE	−10.69	8.13	7.59	18.55	−10.69	16.59	−11.89	−9.29	−10.69	−0.20
FT97	−7.86	10.09	11.41	17.68	−7.86	19.37	−7.85	−6.76	−7.86	−0.04
HCTH/93	−9.37	10.25	6.99	15.53	−9.37	19.56	−11.80	−9.74	−9.37	3.82
HCTH/120	−11.60	7.46	6.03	18.16	−11.60	16.42	−13.03	−9.56	−11.60	−0.49
HCTH/147	−10.89	8.14	6.62	17.62	−10.89	17.15	−12.62	−9.54	−10.89	0.50
HCTH/407	−11.71	8.19	4.55	16.45	−11.71	17.82	−13.88	−9.93	−11.71	1.99
BOP	−9.91	6.83	4.60	13.45	−9.91	15.96	−13.74	−12.01	−9.91	−1.20
OPBE	−8.64	13.99	12.33	20.78	−8.64	22.32	−8.34	−6.24	−8.64	7.56
OLYP	−9.66	10.68	7.45	16.33	−9.66	19.58	−11.81	−9.28	−9.66	4.04
					meta-GGAs					
PKZB	−10.93	11.36	8.73	17.81	−10.93	20.17	−10.07	−7.06	−10.93	1.23
VS98	−14.96	8.52	2.10	14.62	−14.96	17.05	−12.73	−8.46	−14.96	−6.44
BLAP3	−11.24	8.51	3.28	14.65	−11.24	18.94	−13.92	−10.77	−11.24	0.08
OLAP3	−9.92	14.00	6.20	15.82	−9.92	24.53	−11.55	−8.08	−9.92	7.72
TPSS	−10.99	9.34	8.95	20.88	−10.99	17.58	−9.89	−7.01	−10.99	−3.22
M06-L	−14.02	12.92	8.99	25.92	−14.02	22.77	−4.73	−2.25	−14.02	2.63
					Hybrid Functionals					
B3LYP	−10.60	11.00	7.03	17.83	−10.60	21.22	−10.78	−8.53	−10.60	0.92
O3LYP	−9.63	14.78	10.26	19.98	−9.63	24.43	−8.70	−6.19	−9.63	6.39
KMLYP	−10.49	20.85	13.68	26.27	−10.49	32.97	−3.27	−1.21	−10.49	8.45
BHandH	−11.59	18.31	14.43	29.18	−11.59	29.33	−4.38	−1.25	−11.59	5.60
mPBE0KCIS	−10.94	13.10	8.92	21.03	−10.94	23.21	−9.44	−6.45	−10.94	4.26
mPW1K	−9.55	19.65	13.23	23.78	−9.55	31.18	−4.58	−2.41	−9.55	8.20
M05	−11.99	19.83	3.73	21.95	−11.99	23.34	−8.86	−3.70	−11.99	4.64
M05-2X	−8.93	12.58	16.60	18.97	−8.93	28.46	−7.75	−5.67	−8.93	6.84
M06	−12.68	17.33	6.17	22.96	−12.68	23.67	−6.49	−2.92	−12.68	3.36
M06-2X	−12.49	10.65	14.98	22.49	−12.49	30.29	−5.85	−4.74	−12.49	10.73

is treated. This TS energy computed again with our best basis set, aug-cc-pVQZ, varies from 18.30 to 4.93 to 8.91 to 5.54 kcal/mol along HF, MP2, CCSD, and CCSD(T), respectively. Note again that HF clearly overestimates the barrier by 9 kcal/mol (see Table 1). Moreover, the CCSD(T) values are converged as a function of the basis-set size (at aug-cc-pVQZ) to within less than half a kilocalorie per mole (see Table 1).

The *syn*-E2 elimination of $Cl^- + CH_3CH_2Cl$ proceeds via the same reactant complex as the *anti*-E2 elimination, which has been already examined above. The energy of the *syn*-E2 transition state computed at aug-cc-pV(T+*d*)Z is again sensitive to the level at which correlation is treated. It ranges from 44.99 to 31.06 to 35.11 to 30.82 along the series of *ab initio* methods (see Table 2). The CCSD(T) values change by less than 2 kcal/mol going from the aug-cc-pV(D+*d*)Z to the aug-cc-pV(T+*d*)Z basis set (see Table 2) and again do not differ much from the CBS energies.

The S_N2 transition states for reactions 1c and 2c are also found to be quite sensitive to the level at which correlation is treated. Thus, at the HF level, at which Coulomb correlation is not included, the energies of the transition states **1cTS** and **2cTS** computed with our best basis set (aug-cc-pVQZ for X = F and aug-cc-pV(T+*d*)Z for X = Cl) amount to 11.50 and 10.38 kcal/mol, respectively (see Table 1 and 2). Introducing Coulomb correlation into the theoretical treatment substantially lowers the barrier. Thus, along HF, MP2, CCSD, and CCSD(T), the energy of **1cTS** ranges from 11.50 to 3.81 to 4.97 to 1.99 kcal/mol and that of **2cTS** from 10.38 to 8.22 to 8.15 to 5.70 kcal/mol, respectively (see Table 1 and 2). Thus, HF significantly overestimates the overall barriers by some 10 and 5 kcal/mol, respectively. Note again how including the triple excitations in the CCSD calculations reduces the overall barrier by 3.0 and 2.4 kcal/mol, respectively. The three highest-level values are within a range of 3.0 and 2.5 kcal/mol for reactions 1c and 2c, respectively, Furthermore, the CCSD(T) values for **1cTS** are converged as a function of the basis-set size to within 0.4 kcal/mol and again do not differ much from the CBS extrapolated CCSD(T) values.

In conclusion, our best CCSD(T) estimate leads to a relative order in overall barriers (i.e., TS energy relative to reactants) of *anti*-E2 (X = F: −1.33 kcal/mol) < S_N2 (X = F: +1.99 kcal/mol) < *syn*-E2 (X = F: +5.54 kcal/mol) ∼ S_N2 (X = Cl: +5.70 kcal/mol) < *anti*-E2 (X = Cl: +17.92 kcal/mol) < *syn*-E2 (X = Cl: +30.82 kcal/mol). The change in preference from *anti*-E2 for X = F to S_N2 for X = Cl is also recovered in the trend of the *central* barriers. Our benchmark consolidates the G2+ values for the relative energies of **1aRC**, **1aTS**, **1bTS**, and **1cTS** on the PES of

Table 5. Errors in Overall and Central Barriers (in kcal/mol) for Various Density Functionals for the *anti*-E2, *syn*-E2, and S_N2 reactions of $X^- + CH_3CH_2X$ (X = F, Cl) Compared to CCSD(T)[a]

	anti-E2				*syn*-E2				S_N2			
	err. in barr. rel. to R		err. in barr. rel. to RC		err. in barr. rel. to R		err. in barr. rel. to RC		err. in barr. rel. to R		err. in barr. rel. to RC	
method	F	Cl	F	Cl	F	Cl	F	Cl	F	Cl	F	Cl
					LDA							
VWN	−7.21	−12.92	6.03	−10.70	−18.04	−19.37	−7.14	−17.15	−15.66	−10.34	−2.42	−8.12
					GGAs							
BP86	−6.94	−10.71	0.26	−11.15	−13.05	−15.47	−7.40	−15.91	−11.32	−7.62	−4.12	−8.06
BLYP	−10.22	−12.64	−2.98	−12.66	−14.20	−16.78	−8.30	−16.80	−13.26	−9.39	−6.02	−9.41
PW91	−8.25	−11.54	0.88	−10.41	−14.83	−16.60	−7.29	−15.47	−13.38	−8.94	−4.25	−7.81
PBE	−8.03	−11.07	0.77	−10.26	−14.52	−16.07	−7.27	−15.26	−12.72	−8.13	−3.92	−7.32
RPBE	−8.28	−10.14	−1.48	−10.04	−12.93	−14.55	−7.31	−14.45	−10.55	−6.37	−3.75	−6.27
revPBE	−7.50	−9.79	−1.12	−10.20	−12.39	−14.23	−7.25	−14.64	−9.90	−5.90	−3.52	−6.31
FT97	−5.21	−7.83	−0.42	−11.07	−10.34	−11.45	−7.38	−14.69	−9.18	−5.74	−4.39	−8.98
HCTH/93	−5.99	−7.67	−2.23	−9.40	−9.27	−11.26	−6.41	−12.99	−4.51	−1.88	−0.75	−3.61
HCTH/120	−8.52	−10.46	−1.61	−9.96	−12.71	−14.40	−6.91	−13.90	−9.36	−6.19	−2.45	−5.69
HCTH/147	−7.60	−9.78	−1.52	−9.99	−11.77	−13.67	−6.79	−13.88	−8.13	−5.20	−2.05	−5.41
HCTH/407	−9.23	−9.73	−2.70	−9.12	−12.14	−13.00	−6.52	−12.39	−7.77	−3.71	−1.24	−3.10
BOP	−8.65	−11.09	−3.97	−12.28	−11.55	−14.86	−7.99	−16.05	−9.65	−6.90	−4.97	−8.09
OPBE	−1.93	−3.93	1.76	−6.39	−7.61	−8.50	−4.94	−10.96	−2.40	1.86	1.29	−0.60
OLYP	−6.62	−7.24	−1.60	−8.68	−10.47	−11.24	−6.39	−12.68	−6.15	−1.66	−1.13	−3.10
					meta-GGAs							
PKZB	−5.23	−6.56	−1.06	−6.73	−9.47	−10.65	−6.04	−10.82	−9.26	−4.47	−5.09	−4.64
VS98	−12.09	−9.40	−6.28	−5.54	−12.58	−13.77	−7.45	−9.91	−16.05	−12.14	−10.24	−8.28
BLAP3	−7.25	−9.41	−3.70	−9.27	−8.01	−11.88	−5.12	−11.74	−6.87	−5.62	−3.32	−5.48
OLAP3	−3.29	−3.92	−2.05	−5.10	−3.97	−6.29	−2.96	−7.47	0.26	2.02	1.50	0.84
TPSS	−3.93	−8.58	2.46	−8.69	−9.70	−13.24	−4.54	−13.35	−12.02	−8.92	−5.63	−9.03
M06-L	0.10	−5.00	5.15	−2.08	−3.86	−8.05	0.35	−5.13	−4.94	−3.07	0.11	−0.15
					Hybrid Functionals							
B3LYP	−4.05	−6.92	0.26	−7.42	−7.54	−9.60	−4.16	−10.10	−6.00	−4.78	−1.69	−5.28
O3LYP	−1.22	−3.14	1.91	−4.61	−5.14	−6.39	−2.80	−7.86	−1.75	0.69	1.38	−0.78
KMLYP	7.42	2.93	8.57	2.32	2.74	2.15	3.39	1.54	5.55	2.75	6.70	2.14
BHandH	5.23	0.39	9.92	0.88	−1.68	−1.49	2.07	−1.00	0.77	−0.10	5.46	0.39
mPBE0KCIS	−3.11	−4.82	1.47	−4.98	−7.31	−7.61	−3.66	−7.77	−3.14	−1.44	1.44	−1.60
mPW1K	5.59	1.73	5.92	0.18	1.52	0.36	1.36	−1.19	4.25	2.50	4.58	0.95
M05	−2.18	1.91	1.51	2.71	−4.73	−7.48	−1.21	−6.68	−2.80	−1.06	0.89	−0.26
M05-2X	2.32	−5.34	1.86	−7.51	−1.69	−2.36	−2.51	−4.53	1.98	1.14	1.52	−1.03
M06	−0.88	−0.59	2.34	0.99	−4.40	−7.15	−1.56	−5.57	−2.34	−2.34	0.88	−0.76
M06-2X	2.82	−7.27	3.50	−5.88	−1.51	−0.53	−1.16	0.86	3.83	5.03	4.51	6.42

[a] Relative to CCSD(T)/aug-cc-pVQZ benchmark for reactions involving F and relative to CCSD(T)/aug-cc-pV(T + d)Z benchmark for reactions involving Cl. R = reactants, RC = reactant complex.

$F^- + CH_3CH_2F$ computed by Gronert and co-workers,[4h] which agree within 2.3 kcal/mol with our best CCSD(T) estimates.

3.3. Validation of DFT: Mean Absolute Error. Next, we examine the relative energies of stationary points computed with (i) the LDA functional VWN; (ii) the GGA functionals BP86, BLYP, PW91, PBE, RPBE, revPBE, FT97, HCTH/93, HCTH/120, HCTH/147, HCTH/407, BOP, OPBE, and OLYP; (iii) the meta-GGA functionals PKZB, VS98, BLAP3, OLAP3, TPSS, and M06-L; and (iv) the hybrid functionals B3LYP, O3LYP, KMLYP, BHandH, mPBE0KCIS, mPW1K, M05, M05-2X, M06, and M06-2X using the following procedure: (i) all functionals except OLYP are evaluated using the OLYP/ae-TZ2P density computed at the OLYP/TZ2P geometries; (ii) the OLYP functional is evaluated using the OLYP/TZ2P density computed at the OLYP/TZ2P geometries (see Methods section). Extensive previous validation studies have shown that the use of the all-electron ae-TZ2P versus the frozen-core TZ2P basis set leads to differences in relative energies of less than half a kilocalorie per mole.[38] The DFT relative energies for reactions 1 and 2 are collected in Tables 3 and 4, respectively (see Table S2 in the Supporting Information for an overview of *overall barriers together with central barriers* for all of the *anti*-E2, *syn*-E2, and S_N2 reactions of $F^- + CH_3CH_2F$ and $Cl^- + CH_3CH_2Cl$ computed with all our 31 functionals).

Here, we focus on the overall barrier, that is, the difference in energy between the TS and the separate reactants (R), and the central barrier, that is, the difference in energy between the TS and the reactant complex (RC). The overall barrier is decisive for the rate of chemical reactions in the gas phase, in particular, if they occur under low-pressure conditions,[2b,6] whereas the central barrier becomes decisive in the high-pressure regime, when termolecular collisions are sufficiently efficient to cool the otherwise rovibrationally hot reactant complex, causing it to be in thermal equilibrium with the environment.[2b,6]

The performance of the various density functional approaches is assessed by a systematic comparison of the resulting PESs with our CCSD(T)/aug-cc-pVQZ benchmark in the case of reaction 1 (Table 1) and the CCSD(T)/aug-

Table 6. Mean Absolute Errors (MAE) in Overall and Central Barriers (in kcal/mol) for Various Density Functionals for the *anti*-E2, *syn*-E2, and S_N2 reactions of $X^- + CH_3CH_2X$ (X = F, Cl) compared to CCSD(T)[a]

	MAE in *anti*-E2 barr.		MAE in *syn*-E2 barr.		MAE in S_N2 barr.		MAE in barr. X = F		MAE in barr. X = Cl		MAE	
method	rel. to R	rel. to RC	rel. to R	rel. to RC	rel. to R	rel. to RC	rel. to R	rel. to RC	rel. to R	rel. to RC	rel. to R	rel. to RC
						LDA						
VWN	10.07	8.37	18.71	12.15	13.00	5.27	13.64	5.20	14.21	11.99	13.92	8.59
						GGAs						
BP86	8.83	5.71	14.26	11.66	9.47	6.09	10.44	3.93	11.27	11.71	10.85	7.82
BLYP	11.43	7.82	15.49	12.55	11.33	7.72	12.56	5.77	12.94	12.96	12.75	9.36
PW91	9.90	5.65	15.72	11.38	11.16	6.03	12.15	4.14	12.36	11.23	12.26	7.69
PBE	9.55	5.52	15.30	11.27	10.43	5.62	11.76	3.99	11.76	10.95	11.76	7.47
RPBE	9.21	5.76	13.74	10.88	8.46	5.01	10.59	4.18	10.35	10.25	10.47	7.22
revPBE	8.65	5.66	13.31	10.95	7.90	4.92	9.93	3.96	9.97	10.38	9.95	7.17
FT97	6.52	5.75	10.90	11.04	7.46	6.69	8.24	4.06	8.34	11.58	8.29	7.82
HCTH/93	6.83	5.82	10.27	9.70	3.20	2.18	6.59	3.13	6.94	8.67	6.76	5.90
HCTH/120	9.49	5.79	13.56	10.41	7.78	4.07	10.20	3.66	10.35	9.85	10.27	6.75
HCTH/147	8.69	5.76	12.72	10.34	6.67	3.73	9.17	3.45	9.55	9.76	9.36	6.61
HCTH/407	9.48	5.91	12.57	9.46	5.74	2.17	9.71	3.49	8.81	8.20	9.26	5.85
BOP	9.87	8.13	13.21	12.02	8.28	6.53	9.95	5.64	10.95	12.14	10.45	8.89
OPBE	2.93	4.08	8.06	7.95	2.13	0.95	3.98	2.66	4.76	5.98	4.37	4.32
OLYP	6.93	5.14	10.86	9.54	3.91	2.12	7.75	3.04	6.71	8.15	7.23	5.60
						meta-GGAs						
PKZB	5.90	3.90	10.06	8.43	6.87	4.87	7.99	4.06	7.23	7.40	7.61	5.73
VS98	10.75	5.91	13.18	8.68	14.10	9.26	13.57	7.99	11.77	7.91	12.67	7.95
BLAP3	8.33	6.49	9.95	8.43	6.25	4.40	7.38	4.05	8.97	8.83	8.17	6.44
OLAP3	3.61	3.58	5.13	5.22	1.14	1.17	2.51	2.17	4.08	4.47	3.29	3.32
TPSS	6.26	5.58	11.47	8.95	10.47	7.33	8.55	4.21	10.25	10.36	9.40	7.28
M06-L	2.55	3.62	5.96	2.74	4.01	0.13	2.97	1.87	5.37	2.45	4.17	2.16
						Hybrid Functionals						
B3LYP	5.49	3.84	8.57	7.13	5.39	3.49	5.86	2.04	7.10	7.60	6.48	4.82
O3LYP	2.18	3.26	5.77	5.33	1.22	1.08	2.70	2.03	3.41	4.42	3.06	3.22
KMLYP	5.18	5.45	2.45	2.47	4.15	4.42	5.24	6.22	2.61	2.00	3.92	4.11
BHandH	2.81	5.40	1.59	1.54	0.44	2.93	2.56	5.82	0.66	0.76	1.61	3.29
mPBE0KCIS	3.97	3.23	7.46	5.72	2.29	1.52	4.52	2.19	4.62	4.78	4.57	3.49
mPW1K	3.66	3.05	0.94	1.28	3.38	2.77	3.79	3.95	1.53	0.77	2.66	2.36
M05	2.05	2.11	6.11	3.95	1.93	0.58	3.24	1.20	3.48	3.22	3.36	2.21
M05-2X	3.83	4.69	2.03	3.52	1.56	1.28	2.00	1.96	2.95	4.36	2.47	3.16
M06	0.74	1.67	5.78	3.57	2.34	0.82	2.54	1.59	3.36	2.44	2.95	2.02
M06-2X	5.05	4.69	1.02	1.01	4.43	5.47	2.72	3.06	4.28	4.39	3.50	3.72

[a] Relative to CCSD(T)/aug-cc-pVQZ benchmark for reactions involving F and relative to CCSD(T)/aug-cc-pV(T + d)Z benchmark for reactions involving Cl. R = reactants, RC = reactant complex.

cc-pV(T+*d*)Z benchmark in the case of reaction 2 (Table 2). Note that our best CCSD(T) results do not differ much from the CBS extrapolated CCSD(T) values. Thus, they were used (instead of the CBS values) as our benchmark since we prefer to have as little as possible empirical extrapolations in the benchmark reference values. For all 31 functionals, we have computed the errors in the overall and central barriers (see Table 5) and the corresponding mean absolute errors (MAE) relative to the CCSD(T) benchmarks for all model reactions together as well as for certain categories thereof (see Table 6).

It is clear from Tables 5 and 6 that LDA suffers from its notorious overbinding: it yields too-low barriers and too-exothermic complexation and reaction energies (see also Tables 3 and 4). But also many of the GGA (e.g., BLYP, BOP, BP86, PW91, and PBE) and some meta-GGA functionals (VS98 and TPSS) perform more or less equally poorly as LDA: together, these poorly performing functionals have MAE values, for all reactions together, in the range 7−9 kcal/mol for central and 9−14 kcal/mol for overall barriers (see Table 6).

Best overall agreement with our *ab initio* benchmark barriers is obtained by representatives from each of the three categories of functionals, GGA, meta-GGA, and hybrid DFT, with MAEs in central barriers of 4.3 (OPBE), 2.2 (M06-L), and 2.0 kcal/mol (M06), respectively, and MAEs in overall barriers of 4.4 (OPBE), 3.3 (OLAP3), and 1.6 kcal/mol (BHandH), respectively (see Table 6). The top three best functionals is constituted for the central barriers of M06, M06-L, and M05 with MAE values, for all reactions together, of 2.0, 2.2, and 2.2 kcal/mol, respectively, and for the overall barriers of BHandH, M05-2X, and mPW1K with MAE values, for all reactions together, of 1.6, 2.5, and 2.7 kcal/mol, respectively (see Table 6). An important point to note is that the OPBE functional is, not only for all reactions together but also for each individual category of reactions (e.g., *anti*-E2 reactions or reactions with X = F, etc.), in the top regions of performance (MAE in a category typically 1−6 kcal/mol, only for *syn*-E2 it reaches 8.1 kcal/mol) of all functionals studied, and it is the best of all *GGA* functionals. OLYP (7.2 and 5.6 kcal/mol relative to R and RC) and B3LYP (6.5 and 4.8 kcal/mol relative to R and RC) are of comparable quality, and both have somewhat larger MAE values for all reactions together than OPBE (4.4 and 4.3 kcal/mol relative to R and RC; see Table 6). OLYP (MAE for S_N2: 3.9 and 2.1 kcal/mol relative to R and RC)

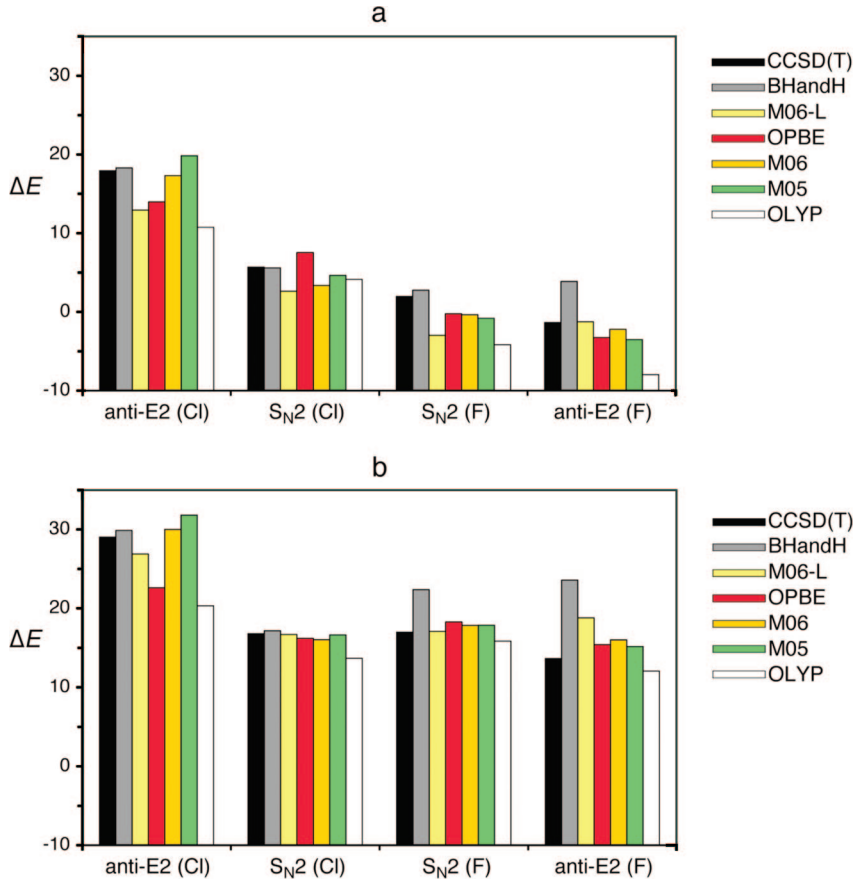

Figure 3. Overall (a) and central (b) barriers (in kcal/mol) for the *anti*-E2 and S_N2 reactions of $X^- + CH_3CH_2X$ (X = F, Cl), computed with CCSD(T) and selected density functionals.

is however slightly better than B3LYP (MAE for S_N2: 5.4 and 3.5 kcal/mol relative to R and RC) for the category of S_N2 reactions (see Table 6), in agreement with previous work.[7a]

Finally, complexation energies of the reactant complexes relative to reactants as well as reaction energies of our model reactions appear to be, in general, somewhat less dependent on the level of both ab initio (see Tables 1 and 2) and density functional theory (see Tables 3–6) if compared with the relative energies of the transition states discussed above. The density functionals that perform best for reaction barriers in terms of MAE, namely, BHandH, M06, M06-L, M05, M05-2X, and mPW1K, also show satisfactory agreement with the CCSD(T) benchmark regarding these complexation and reaction energies, with MAEs in the range of 0.7−4.8 kcal/mol (values not shown in Table 6). OPBE and B3LYP also achieve MAE values within this range, whereas OLYP has MAE values of 3.5 and 6.0 kcal/mol for complexation and reaction energies, respectively.

3.4. Validation of DFT: Trends. So far, we have concentrated on the MAE, which leads to a certain ranking of density functionals regarding their performance in computing overall or central barriers for the six model reaction pathways (see Scheme 2). Interestingly (and importantly), such an MAE-based ranking does not necessarily say something about the performance for reproducing the right trends in reactivity.

For example, according to the MAE criterion, BHandH and M06-L belong to the best functionals. Yet, they erroneously predict that, for $F^- + CH_3CH_2F$, the *anti*-E2 reaction has both a higher overall and central barrier than the S_N2 reaction, as can be seen in Figure 3a and b, respectively (see also Tables 3 and 4). For comparison, both OPBE and OLYP do reproduce the correct trend (see Figure 3), in spite of the fact that the MAE is larger than that for BHandH or M06-L (see Table 6). In the latter two functionals, the error is apparently somewhat less uniformly distributed. This is an interesting phenomenon, but it should also not be overrated because the energy differences concerned are rather small.

M06 and M05 are good both in terms of one of the smallest MAE values (see Table 6) and a correct trend in reactivity (see Figure 3 and Tables 3 and 4). On the other hand, they are computationally somewhat more expensive than OPBE and OLYP. And, at variance with the latter, M06 and M05 are (in ADF) evaluated post-SCF with the density of another potential (e.g., OPBE or OLYP).

4. Conclusions

We have computed *ab initio* benchmarks for the archetypal competing E2 and S_N2 reactions of fluoride + fluoroethane and chloride + chloroethane. These benchmarks derive from hierarchical series of methods up to CCSD(T)/aug-cc-pVQZ (up to CCSD(T)/aug-cc-pV(T+*d*)Z for chloride + chloro-

ethane), which are converged with respect to the basis-set size within less than half a kilocalorie per mole. The resulting reaction profiles show that *anti*-E2 dominates for $F^- + CH_3CH_2F$ while S_N2 dominates for $Cl^- + CH_3CH_2Cl$. This change in preference is reflected by both overall and central barriers. On the other hand, *syn*-E2 is in both reaction systems the least favorable pathway.

Our *ab initio* benchmark is used to evaluate the performance of 31 density functionals for describing the above *anti*-E2, *syn*-E2, and S_N2 reactions. The best overall agreement regarding central reaction barriers with our *ab initio* benchmark is obtained by representatives from each of the three categories of functionals, GGA, meta-GGA, and hybrid DFT, with mean absolute errors of 4.3 (OPBE), 2.2 (M06-L), and 2.0 kcal/mol (M06), respectively.

Importantly, the hybrid functional BHandH and the meta-GGA M06-L yield incorrect trends and qualitative features of the PESs (in particular, an erroneous preference for S_N2 over the *anti*-E2 in the case of $F^- + CH_3CH_2F$) even though they are among the best functionals as measured by their small mean absolute errors of 3.3 and 2.2 kcal/mol in reaction barriers. OLYP and B3LYP have somewhat higher mean absolute errors in central barriers (5.6 and 4.8 kcal/mol, respectively), but the error distribution is somewhat more uniform, and as a consequence, the correct trends are reproduced.

Acknowledgment. We thank The Netherlands Organization for Scientific Research (NWO-CW), the European HPC-Europa program, the Spanish Ministerio de Educación y Cultura (MEC), and the Catalan DURSI (Generalitat de Catalunya) for financial support. Excellent service by the Stichting Academisch Rekencentrum Amsterdam (SARA) and the Centre de Supercomputació de Catalunya (CESCA) is gratefully acknowledged.

Supporting Information Available: Cartesian coordinates of all stationary points. This material is available free of charge via the Internet at http://pubs.acs.org.

References

(1) (a) Smith, M. B.; March, J. *March's Advanced Organic Chemistry: Reactions, Mechanisms, and Structure*; Wiley: New York, 2007. (b) Carey, F. A.; Sundberg, R. J. *Advanced Organic Chemistry, Part A*; Plenum Press: New York, 1984. (c) Ingold, C. K. *Structure and Mechanism in Organic Chemistry*; Cornell University Press: Ithaca, NY, 1969. (d) Lowry, T. H.; Richardson, K. S. *Mechanism and Theory in Organic Chemistry*, 3rd ed.; Harper and Row: New York, 1987.

(2) (a) Gronert, S. *Chem. Rev.* **2001**, *101*, 329. (b) Bickelhaupt, F. M. *Mass Spectrom. Rev.* **2001**, *20*, 347. (c) Gronert, S.; Pratt, L. M.; Mogali, S. *J. Am. Chem. Soc.* **2001**, *123*, 3081. (d) Gronert, S. *Acc. Chem. Res.* **2003**, *36*, 848. (e) Bickelhaupt, F. M.; de Koning, L. J.; Nibbering, N. M. M. *J. Org. Chem.* **1993**, *58*, 2436. (f) Uggerud, E.; Bache-Andreassen, L. *Chem.—Eur. J.* **1999**, *5*, 1917. (g) Gronert, S.; Fagin, A. E.; Okamoto, K.; Mogali, S.; Pratt, L. M. *J. Am. Chem. Soc.* **2004**, *126*, 12977. (h) Villano, S. M.; Kato, S.; Bierbaum, V. M. *J. Am. Chem. Soc.* **2006**, *128*, 736. (i) Bickelhaupt, F. M.; Buisman, G. J. H.; de Koning, L. J.; Nibbering, N. M. M.; Baerends, E. J. *J. Am. Chem. Soc.* **1995**, *117*, 9889. (j) Flores, A. E.; Gronert, S. *J. Am. Chem. Soc.* **1999**, *121*, 2627. (k) DePuy, C. H.; Gronert, S.; Mullin, A.; Bierbaum, V. M. *J. Am. Chem. Soc.* **1990**, *112*, 8650.

(3) (a) Orita, A.; Otera, J. *Chem. Rev.* **2006**, *106*, 5387. (b) Alunni, S.; De Angelis, F.; Ottavi, L.; Papavasileiou, M.; Tarantelli, F. *J. Am. Chem. Soc.* **2005**, *127*, 15151. (c) Meng, Q.; Thibblin, A. *J. Am. Chem. Soc.* **1995**, *117*, 9399. (d) Pirinccioglu, N.; Thibblin, A. *J. Am. Chem. Soc.* **1998**, *120*, 6512.

(4) (a) Bickelhaupt, F. M. *J. Comput. Chem.* **1999**, *20*, 114. (b) Ensing, B.; Laio, A.; Gervasio, F. L.; Parrinello, M.; Klein, M. L. *J. Am. Chem. Soc.* **2004**, *126*, 9492. (c) De Angelis, F.; Tarantelli, F.; Alunni, S. *J. Phys. Chem. B* **2006**, *110*, 11014. (d) Almerindo, G. I.; Pliego, R., Jr *Org. Lett.* **2005**, *7*, 1821. (e) Ensing, B.; Klein, M. L. *Proc. Natl. Acad. Sci. U.S.A.* **2005**, *102*, 6755. (f) Chung, D. S.; Kim, C. K.; Lee, B.-S.; Lee, I. *J. Phys. Chem. A* **1997**, *101*, 9097. (g) Merrill, G. N.; Gronert, S.; Kass, S. R. *J. Phys. Chem. A* **1997**, *101*, 208. (h) Gronert, S. *J. Org. Chem.* **1995**, *60*, 488. (i) Minato, T.; Yamabe, S. *J. Am. Chem. Soc.* **1985**, *107*, 4621. (j) Minato, T.; Yamabe, S. *J. Am. Chem. Soc.* **1988**, *110*, 4586. (k) Gronert, S. *J. Am. Chem. Soc.* **1993**, *115*, 652. (l) Gronert, S. *J. Am. Chem. Soc.* **1991**, *113*, 6041.

(5) (a) Bach, R. D.; Glukhovtsev, M. N.; Gonzales, C. *J. Am. Chem. Soc.* **1998**, *120*, 9902. (b) Baker, J.; Muir, M.; Andzelm, J. *J. Chem. Phys.* **1995**, *102*, 2063. (c) Baker, J.; Pulay, P. *J. Chem. Phys.* **2002**, *117*, 1441. (d) Barone, V.; Adamo, C. *J. Chem. Phys.* **1996**, *105*, 11007. (e) Gritsenko, O. V.; Ensing, B.; Schippers, P. R. T.; Baerends, E. J. *J. Phys. Chem. A* **2000**, *104*, 8558. (f) Poater, J.; Solà, M.; Duran, M.; Robles, J. *Phys. Chem. Chem. Phys.* **2002**, *4*, 722. (g) Thümmel, H. T.; Bauschlicher, C. W. *J. Phys. Chem. A* **1997**, *101*, 1188. (h) Diefenbach, A.; Bickelhaupt, F. M. *J. Chem. Phys.* **2001**, *115*, 4030.

(6) (a) Nibbering, N. M. M. *Adv. Phys. Org. Chem.* **1988**, *24*, 1. (b) Nibbering, N. M. M. *Acc. Chem. Res.* **1990**, *23*, 279.

(7) (a) Bento, A. P.; Solà, M.; Bickelhaupt, F. M. *J. Comput. Chem.* **2005**, *26*, 1497. (b) Swart, M.; Solà, M.; Bickelhaupt, F. M. *J. Comput. Chem.* **2007**, *28*, 1551. (c) Swart, M.; Ehlers, A. W.; Lammertsma, K. *Mol. Phys.* **2004**, *102*, 2467. (d) Xu, X.; Goddard, W. A., III *J. Phys.Chem. A* **2004**, *108*, 8495. (e) Gonzales, J. M.; Allen, W. D.; Schaefer, H. F., III *J. Phys. Chem. A* **2005**, *109*, 10613. (f) Gonzales, J. M.; Pak, C.; Cox, R. S.; Allen, W. D.; Schaefer, H. F., III; Császár, A. G.; Tarczay, G. *Chem.—Eur. J.* **2003**, *9*, 2173. (g) Guner, V. A.; Khuong, K. S.; Houk, K. N.; Chuma, A.; Pulay, P. *J. Phys. Chem. A* **2004**, *108*, 2959. (h) Zhao, Y.; Truhlar, D. G. *Acc. Chem. Res.* **2008**, *41*, 157.

(8) (a) Baerends, E. J.; Autschbach, J.; Bérces, A.; Berger, J. A.; Bickelhaupt, F. M.; Bo, C.; de Boeij, P. L.; Boerrigter, P. M.; Cavallo, L.; Chong, D. P.; Deng, L.; Dickson, R. M.; Ellis, D. E.; van Faassen, M.; Fan, T.; Fischer, T. H.; Fonseca Guerra, C.; van Gisbergen, S. J. A.; Groeneveld, J. A.; Gritsenko, O. V.; Grüning, M.; Harris, F. E.; van den Hoek, P.; Jacob, C. R.; Jacobsen, H.; Jensen, L.; Kadantsev, E. S.; van Kessel, G.; Klooster, R.; Kootstra, F.; van Lenthe, E.; McCormack, D. A.; Michalak, A.; Neugebauer, J.; Nicu, V. P.; Osinga, V. P.; Patchkovskii, S.; Philipsen, P. H. T.; Post, D.; Pye, C. C.; Ravenek, W.; Romaniello, P.; Ros, P.; Schipper, P. R. T.; Schreckenbach, G.; Snijders, J.; Solà, M.; Swart, M.; Swerhone, D.; te Velde, G.; Vernooijs, P.; Versluis, L.; Visscher, L.; Visser, O.; Wang, F.; Wesolowski, T. A.; van Wezenbeek, E. M.; Wiesenekker, G.; Wolff, S. K.; Woo, T. K.; Yakovlev, A. L.; Ziegler, T. *ADF200701*; SCM: Amsterdam, The Netherlands. (b) te Velde, G.; Bickelhaupt,

F. M.; Baerends, E. J.; Fonseca Guerra, C.; van Gisbergen, S. J. A.; Snijders, J. G.; Ziegler, T. *J. Comput. Chem.* **2001**, *22*, 931. (c) Fonseca Guerra, C.; Snijders, J. G.; te Velde, G.; Baerends, E. J. *Theor. Chem. Acc.* **1998**, *99*, 391.

(9) (a) Handy, N. C.; Cohen, A. J. *Mol. Phys.* **2001**, *99*, 403. (b) Lee, C.; Yang, W.; Parr, R. G. *Phys. Rev. B: Condens. Matter Mater. Phys.* **1988**, *37*, 785.

(10) Baerends, E. J.; Ellis, D. E.; Ros, P. *Chem. Phys.* **1973**, *2*, 41.

(11) Fan, L.; Ziegler, T. *J. Chem. Phys.* **1990**, *92*, 3645.

(12) Fan, L.; Versluis, L.; Ziegler, T.; Baerends, E. J.; Ravenek, W. *Int. J. Quantum Chem., Quantum Chem. Symp.* **1988**, *S22*, 173.

(13) Vosko, S. H.; Wilk, L.; Nusair, M. *Can. J. Phys.* **1980**, *58*, 1200.

(14) (a) Becke, A. D. *Phys. Rev. A: At., Mol., Opt. Phys.* **1988**, *38*, 3098. (b) Perdew, J. P. *Phys. Rev. B: Condens. Matter Mater. Phys.* **1986**, *33*, 8822.

(15) (a) Perdew, J. P. In *Electronic Structure of Solids*; Ziesche, P., Eschrig, H., Eds.; Akademie Verlag: Berlin, 1991. (b) Perdew, J. P.; Chevary, J. A.; Vosko, S. H.; Jackson, K. A.; Pederson, M. R.; Singh, D. J.; Fiolhais, C. *Phys. Rev. B: Condens. Matter Mater. Phys.* **1992**, *46*, 6671. (Erratum: *Ibid.* **1993**, *48*, 4978).

(16) Perdew, J. P.; Burke, K.; Ernzerhof, M. *Phys. Rev. Lett.* **1996**, *77*, 3865. (Erratum: *Ibid.* **1997**, *78*, 1396)

(17) Hammer, B.; Hansen, L. B.; Nørskov, J. K. *Phys. Rev. B: Condens. Matter Mater. Phys.* **1999**, *59*, 7413.

(18) Zhang, Y.; Yang, W. *Phys. Rev. Lett.* **1998**, *80*, 890.

(19) Filatov, M.; Thiel, W. *Mol. Phys.* **1997**, *91*, 847.

(20) Hamprecht, F. A.; Cohen, A. J.; Tozer, D. J.; Handy, N. C. *J. Chem. Phys.* **1998**, *109*, 6264.

(21) Boese, A. D.; Doltsinis, N. L.; Handy, N. C.; Sprik, M. *J. Chem. Phys.* **2000**, *112*, 1670.

(22) Boese, A. D.; Handy, N. C. *J. Chem. Phys.* **2001**, *114*, 5497.

(23) Tsuneda, T.; Suzumura, T.; Hirao, K. *J. Chem. Phys.* **1999**, *110*, 10664.

(24) (a) Perdew, J. P.; Kurth, S.; Zupan, A.; Blaha, P. *Phys. Rev. Lett.* **1999**, *82*, 2544. (Erratum: *Ibid.* **1999**, *82*, 5179)

(25) Van Voorhis, T.; Scuseria, G. E. *J. Chem. Phys.* **1998**, *109*, 400.

(26) Proynov, E. I.; Sirois, S.; Salahub, D. R. *Int. J. Quantum Chem.* **1997**, *64*, 427.

(27) (a) Tao, J.; Perdew, J. P.; Staroverov, V. N.; Scuseria, G. E. *Phys. Rev. Lett.* **2003**, *91*, 146401. (b) Staroverov, V. N.; Scuseria, G. E.; Tao, J.; Perdew, J. P. *J. Chem. Phys.* **2003**, *119*, 12129. (Erratum: *Ibid.* **2004**, *121*, 11507)

(28) Zhao, Y.; Truhlar, D. G. *J. Chem. Phys.* **2006**, *125*, 194101.

(29) Becke, A. D. *J. Chem. Phys.* **1993**, *98*, 5648.

(30) Cohen, A. J.; Handy, N. C. *Mol. Phys.* **2001**, *99*, 607.

(31) Kang, J. K.; Musgrave, C. B. *J. Chem. Phys.* **2001**, *115*, 11040.

(32) Becke, A. D. *J. Chem. Phys.* **1993**, *98*, 1372.

(33) Toulouse, J.; Adamo, C. *Chem. Phys. Lett.* **2002**, *362*, 72.

(34) Lynch, B. J.; Fast, P. L.; Harris, M.; Truhlar, D. G. *J. Phys. Chem. A* **2000**, *104*, 4811.

(35) Zhao, Y.; Schultz, N. E.; Truhlar, D. G. *J. Chem. Phys.* **2005**, *123*, 161103.

(36) Zhao, Y.; Schultz, N. E.; Truhlar, D. G. *J. Chem. Theory Comput* **2006**, *2*, 364.

(37) Zhao, Y.; Truhlar, D. G. *Theor. Chem. Acc.* **2008**, *120*, 215. (Erratum: *Ibid.* **2008**, *119*, 525).

(38) (a) Swart, M.; Groenhof, A. R.; Ehlers, A. W.; Lammertsma, K. *J. Phys. Chem. A* **2004**, *108*, 5479. (b) de Jong, G. Th.; Bickelhaupt, F. M. *J. Chem. Theory Comput.* **2006**, *2*, 322. (c) de Jong, G. Th.; Bickelhaupt, F. M. *J. Phys. Chem. A* **2005**, *109*, 9685. (d) de Jong, G. Th.; Geerke, D. P.; Diefenbach, A.; Solà, M.; Bickelhaupt, F. M. *J. Comput. Chem.* **2005**, *26*, 1006. (e) de Jong, G. Th.; Geerke, D. P.; Diefenbach, A.; Bickelhaupt, F. M. *Chem. Phys.* **2005**, *313*, 261.

(39) Frisch, M. J.; Trucks, G. W.; Schlegel, H. B.; Scuseria, G. E.; Robb, M. A.; Cheeseman, J. R.; Montgomery, J. A., Jr.; Vreven, T.; Kudin, K. N.; Burant, J. C.; Millam, J. M.; Iyengar, S. S.; Tomasi, J.; Barone, V.; Mennucci, B.; Cossi, M.; Scalmani, G.; Rega, N.; Petersson, G. A.; Nakatsuji, H.; Hada, M.; Ehara, M.; Toyota, K.; Fukuda, R.; Hasegawa, J.; Ishida, M.; Nakajima, T.; Honda, Y. ; Kitao, O.; Nakai, H.; Klene, M.; Li, X.; Knox, J. E.; Hratchian, H. P.; Cross, J. B.; Bakken, V.; Adamo, C.; Jaramillo, J.; Gromperts, R.; Stratmann, R. E.; Yazyev, O.; Austin, A. J.; Cammi, R.; Pomelli, C.; Ochterski, J. W.; Ayala, P. Y.; Morokuma, K.; Voth, G. A.; Salvador, P.; Dannenberg, J. J.; Zakrzewski, G.; Dapprich, S.; Daniels, A. D.; Strain, M. C.; Farkas, O.; Malick, D. K.; Rabuck, A. D.; Raghavachari, K.; Foresman, J. B.; Ortiz, J. V.; Cui, Q.; Baboul, A. G.; Clifford, S.; Cioslowski, J.; Stefanov, B. B.; Liu, G.; Liashenko, A.; Piskorz, P.; Komaromi, I.; Martin, R. L.; Fox, D. J.; Keith, T.; Al-Laham, M. A.; Peng, C. Y.; Nanayakkara, A.; Challacombe, M.; Gill, P. M. W.; Johnson, B.; Cheng, W.; Wong, M. W.; Gonzalez, C.; Pople, J. A. *Gaussian 03*; Gaussian Inc.: Pittsburgh, PA, 2003.

(40) Møller, C.; Plesset, M. S. *Phys. Rev.* **1934**, *46*, 618.

(41) (a) Krishnan, R.; Pople, J. A. *Int. J. Quantum Chem.* **1978**, *14*, 91. (b) Krishnan, R.; Frisch, M. J.; Pople, J. A. *J. Chem. Phys.* **1980**, *72*, 4244.

(42) Cizek, J. *J. Chem. Phys.* **1966**, *45*, 4256.

(43) Purvis, G. D., III; Bartlett, R. J. *J. Chem. Phys.* **1982**, *76*, 1910.

(44) Raghavachari, K.; Trucks, G. W.; Pople, J. A.; Head-Gordon, M. *Chem. Phys. Lett.* **1989**, *157*, 479.

(45) (a) Dunning, T. H., Jr *J. Chem. Phys.* **1989**, *90*, 1007. (b) Kendall, R. A.; Dunning, T. H., Jr.; Harrison, R. J. *J. Chem. Phys.* **1992**, *96*, 6796. (c) Dunning, T. H., Jr.; Peterson, K. A.; Wilson, A. K. *J. Chem. Phys.* **2001**, *114*, 9244. (d) The aug-cc-pV(n + d)Z basis set was obtained from the Extensible Computational Chemistry Environment Basis Set Database, Version 02/02/06, as developed and distributed by the Molecular Science Computing Facility, Environmental and Molecular Sciences Laboratory, which is part of the Pacific Northwest Laboratory, P.O. Box 999, Richland, WA 99352, and funded by the U.S. Department of Energy.

(46) Halkier, A.; Helgaker, T.; Jørgensen, P.; Klopper, W.; Koch, H.; Olsen, J.; Wilson, A. K. *Chem. Phys. Lett.* **1998**, *286*, 243.

CT700318E